RSC Advances

PAPER

View Article Online
View Journal | View Issue

Cite this: *RSC Adv.*, 2025, **15**, 48544

Structure-dependent pyrolysis mechanisms of tobacco carbohydrates: from monosaccharides to polysaccharides under programmed and fast pyrolysis conditions

Yuhan Peng,[a] Xiaopeng Shi,[b] Xiaodong Tang,[a] Lu Dai,[a] Depo Cao,[a] Qingxiang Li,[a] Fangqi Du,[a] Kaige Wang *[b] and Yiming Bi*[a]

This study systematically investigates the pyrolysis mechanisms of typical carbohydrates in tobacco under both fast pyrolysis (500 °C) and temperature-programmed conditions (50–500 °C), with a focus on their structural influences on product distributions and reaction pathways. Comparing the fast and temperature-programmed pyrolysis experiments reveals the pyrolysis pathways and product distributions of different structural sugars. Using Py-GC/MS analysis, we demonstrate that small-molecule sugars exhibit distinct pyrolysis behaviors: glucose favors diversified products through 1,2-enolization, while fructose preferentially forms furans *via* 2,3-enolization due to its ketose configuration. Macromolecular sugars display structure-dependent mechanisms: cellulose yields anhydrosugars through β-1,4-glycosidic cleavage; amylose's α-1,4-linked helical structure enhances anhydrosugar production (62.21%); and xylan's pentose units promote furfural selectivity (46.6%). The Maillard reaction with proline significantly alters pyrolysis pathways, introducing nitrogenous heterocycles and suppressing anhydrosugars while enhancing the ester formation. These findings elucidate the structure–activity relationships governing tobacco carbohydrate pyrolysis, offering a theoretical foundation for optimizing pyrolysis processes and developing functional flavor compounds.

Received 23rd September 2025
Accepted 3rd November 2025

DOI: 10.1039/d5ra07210g

rsc.li/rsc-advances

1 Introduction

The main chemical components of tobacco include cellulose, hemicellulose, lignin, proteins, carbohydrates, nicotine, polyphenols, volatile organic acids, and hydrocarbon compounds.[1–3] These components not only constitute the primary chemical framework of tobacco leaves but also play a crucial role in pyrolysis, influencing the types and distribution of final pyrolysis products.[4–6] During pyrolysis, these components undergo a series of complex thermochemical reactions, generating various gaseous and liquid products that significantly impact the aroma profile and sensory characteristics of tobacco smoke.[7,8] Cellulose and hemicellulose, as the dominant carbohydrate constituents in tobacco, primarily decompose into small-molecule compounds such as furans, aldehydes, ketones, and carboxylic acids during pyrolysis.[9,10] Among these, furan derivatives contribute distinct caramel and nutty notes, enhancing the sweet aroma of tobacco smoke, while aldehydes and ketones impart fruity and mild aromatic qualities.[11] Additionally, cellulose pyrolysis yields small amounts of carboxylic acids, which can react with alkaline components to modulate the pH balance of smoke, thereby influencing the sensory experience during smoking.[12] Phenolic compounds contribute to a rich, characteristic smoky aroma, while aromatic aldehydes such as vanillin provide sweet and warm flavor nuances, serving as key aroma sources in tobacco smoke.[13]

Proteins, as the primary source of nitrogenous compounds in tobacco, predominantly generate pyrazines, pyridines, and indoles upon pyrolysis.[14] Pyrazines impart nutty and roasted flavors, while pyridines contribute a characteristic bitter note—an appropriate level enriches the smoke's complexity, whereas excess may cause irritation.[15] Protein pyrolysis may also produce nitrogen-containing gases such as ammonia and nitriles, which participate in subsequent reactions and exert complex effects on the overall aroma profile.[16,17] Furthermore, the partial pyrolysis of nicotine yields pyridine derivatives, while its undecomposed fraction directly contributes to the smoke's irritancy and bitter characteristics.[18] Volatile organic acids and hydrocarbons generate small-molecule acids and aromatic hydrocarbons during pyrolysis, enriching the smoke's aromatic complexity and sweetness while modulating its irritancy.[19,20]

Examining the pyrolysis interaction mechanisms among tobacco components can elucidate the influence of different

[a]*China Tobacco Zhejiang Industrial Co., Ltd, Hangzhou 310008, China. E-mail: 849679720@qq.com*

[b]*State Key Laboratory of Clean Energy Utilization, Zhejiang University, Hangzhou 310027, China. E-mail: kaigewang@zju.edu.cn*

pyrolysis conditions (*e.g.*, temperature, atmosphere, and heating rate) on reaction pathways and product distribution. For instance, under an inert atmosphere, the co-pyrolysis of cellulose and lignin tends to favor the formation of volatile small molecules, while in an oxidative environment, polyphenolic compounds may preferentially undergo oxidation, altering the reaction equilibrium of the system.[21,22] The pyrolysis pathways of carbohydrates are closely correlated with their molecular structures. Previous studies[23] have demonstrated that the pyrolysis mechanisms of monosaccharides differ significantly from those of polysaccharides, leading to distinct product distributions. For instance, polysaccharides such as cellulose primarily undergo depolymerization to generate levoglucosan, whereas monosaccharides such as glucose tend to decompose through fragmentation reactions to produce smaller furans and carbonyl compounds. Such mechanistic studies not only enhance the fundamental understanding of tobacco leaf pyrolysis but also provide theoretical support for industrial applications aimed at optimizing smoke characteristics through controlled pyrolysis conditions. Investigating the interaction mechanisms of pyrolysis reactions among key tobacco components is crucial for uncovering the underlying reaction principles of tobacco pyrolysis systems. Most existing studies have primarily focused on individual carbohydrate or simple model compounds, lacking a systematic comparison of the pyrolytic behaviors of structurally distinct carbohydrates under controlled temperature conditions.

To systematically investigate the pyrolysis behavior of different tobacco constituents, an advanced pyrolysis setup was employed in this study, distinguishing it from conventional experimental approaches. By comparing programmed and rapid pyrolysis processes, qualitative and semi-quantitative analyses were conducted on representative carbohydrate components in tobacco. The study elucidates the specific product formation pathways and distribution patterns of various sugar-derived intermediates during pyrolysis, with particular emphasis on the structure and product relationship between individual components and their characteristic pyrolysis products. This work provides a comprehensive understanding of the pyrolysis routes and underlying mechanisms, thereby offering a scientific basis for optimizing tobacco pyrolysis processes and improving the quality of pyrolysis-derived products.

2 Materials and methods

2.1 Materials

The following chemicals were used in this study: glucose (analytical purity ≥99.90%, Shanghai Rhawn Chemical Technology Co., Ltd), fructose (analytical purity ≥99.90%, Shanghai Rhawn Chemical Technology Co., Ltd), microcrystalline cellulose (biochemical purity ≥ 98.00%, Shanghai Yuanye Bio-Technology Co., Ltd), amylose (from potato, purity ≥ 99.00%, Shanghai Rhawn Chemical Technology Co., Ltd), proline (analytical purity ≥ 99.0%, Shanghai Rhawn Chemical Technology Co., Ltd), and xylan (from beechwood, purity ≥ 95.00%, Shanghai Rhawn Chemical Technology Co., Ltd). All reagents were used as received without further purification.

2.2 Pyrolysis experiments

2.2.1 Fast pyrolysis experiments. Fast pyrolysis experiments were performed using a micro-pyrolyzer coupled with a gas chromatography-mass spectrometer (Agilent 8860/5977B).[24] The reaction zone was preheated to 500 °C prior to sample introduction. Samples (0.50 mg) were precisely weighed into sample cups and rapidly introduced into the preheated zone. The pyrolysis reaction was maintained at 500 °C for 10 minutes to ensure complete devolatilization and thorough reaction.

Ultra-high purity helium (>99.99%) served as the carrier gas to maintain an inert atmosphere throughout the process. The evolved pyrolysis vapors were immediately transferred to the GC-MS system. Chromatographic separation was achieved using a DB-5HT capillary column (30 m × 0.25 mm × 0.25 μm) with a temperature program starting at 40 °C (2 min hold), then ramping to 240 °C at 6°C min^{-1} (5 min final hold). Compound identification was accomplished by comparing mass spectra with the NIST 20.L library. Relative content (%) was defined as the percentage of the GC/MS total ion chromatogram (TIC) peak area of each identified compound relative to the sum of all identified peaks within the same experiment (for fast pyrolysis) or within the same temperature stage (for temperature-programmed pyrolysis).

2.2.2 Temperature-programmed pyrolysis experiments. Except for the heating program, the temperature-programmed runs used the same micro-pyrolyzer GC/MS platform as in Section 2.2.1 (Agilent 8860/5977B) with identical transfer-line and GC conditions; a cooled focusing module was employed to collect volatiles from each stage. For temperature-programmed pyrolysis analysis, a multi-stage heating protocol was implemented: (1) initial heating from 50 °C to 200 °C at 20°C min^{-1} with a 15 min isothermal period, (2) subsequent heating to 325 °C at the same rate with another 15 min hold, and (3) final heating to 500 °C followed by a 15 min isothermal stage. Between each temperature stage, the system was purged with inert gas to prevent cross-contamination. Volatile products from each stage were cryogenically trapped using a liquid nitrogen-cooled focusing module (−100 °C) for 5 min before thermal desorption and GC-MS analysis. This approach enabled stage-wise characterization of products across temperature windows.

3 Results and discussion

3.1 Mechanism of fast pyrolysis for small-molecule sugar compounds

Glucose and fructose, as the predominant reducing sugars in tobacco, significantly influence cigarette aroma and taste through their content and transformation degrees.[25] Fig. 1 shows that fast pyrolysis of glucose primarily yields furfural, levoglucosan (LVG), and 5-hydroxymethylfurfural (HMF) (16%, 27%, 30%, respectively). Under elevated temperatures, glucose undergoes dehydration and rearrangement reactions to form these oxygenated heterocyclic compounds. The pyrolytic mechanism initiates with the ring opening of glucose to form linear intermediates, followed by isomerization to fructose

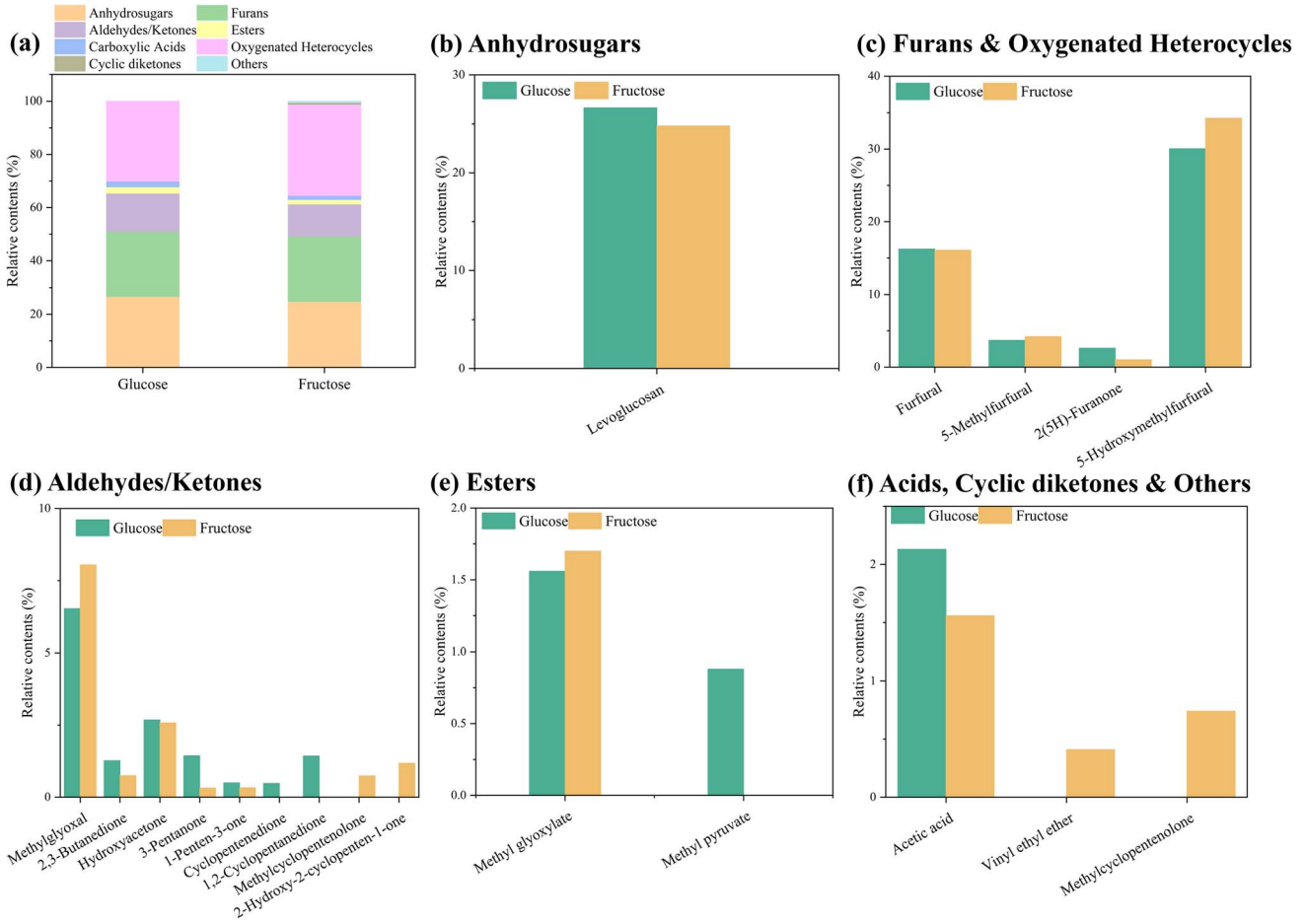

Fig. 1 Product distributions after the fast pyrolysis of small-molecule sugars: (a) overall product distributions of glucose and fructose; (b) anhydrosugars; (c) furans and oxygenated heterocycles; (d) aldehydes/ketones; (e) esters; (f) acids, cyclic diketones and other compounds.

derivatives.[26] Subsequent dehydration and dehydrogenation of these intermediates generate characteristic products, including furfural and HMF. The vigorous fast pyrolysis conditions promote extensive dehydration, producing substantial LVG that subsequently fragments into smaller carbonyl compounds. Furfural formation involves C–C bond cleavage and cyclization to stable furan structures, while smaller fragments yield low-molecular-weight species such as formic acid and glycolaldehyde.

Fructose, a crucial water-soluble monosaccharide constituting 6–8% of dry tobacco weight, participates in complex thermal reactions during combustion and pyrolysis. GC-MS analysis reveals that fructose pyrolysis preferentially generates HMF (34.27%) compared to glucose (30.06%), while producing less LVG (24.81% *vs.* 26.66% for glucose). This disparity stems from fructose's inherent furanose configuration, which facilitates more efficient and selective HMF formation under milder conditions.[27,28] The conversion of glucose to HMF requires preliminary isomerization to fructose, a process limited by ~50% equilibrium conversion efficiency, thereby constraining ultimate HMF yield.

The distinct product distributions reflect fundamental structural differences: fructose pyrolysis predominantly yields furan derivatives due to rapid bond scission of its hydroxyl and carbonyl groups under flash heating, whereas glucose generates more diverse products, including pyran derivatives, ketones, alcohols, and gaseous fragments. This product complexity arises from glucose's multiple reactive hydroxyl groups and aldehyde functionality under combined thermal and kinetic effects. Consequently, fast pyrolysis of glucose produces a broader spectrum of compounds with more balanced distribution ratios compared to the more concentrated product profile from fructose.

3.2 Mechanism of temperature-programmed pyrolysis for small-molecule sugar compounds

Fig. 2 illustrates the product distribution from the temperature-programmed pyrolysis of glucose. In the low-temperature range (50–200 °C), LVG emerged as the dominant product, with a relative abundance of 65.12%, indicating preferential formation of stable cyclic structures through dehydration reactions at mild temperatures. Notably, HMF was also significantly produced (29.92%), demonstrating its generation *via* dehydration and rearrangement pathways within this temperature window. The minor presence of furfural (4.95%) likely originated from secondary decomposition of HMF. A distinct temperature-dependent evolution was observed, showing

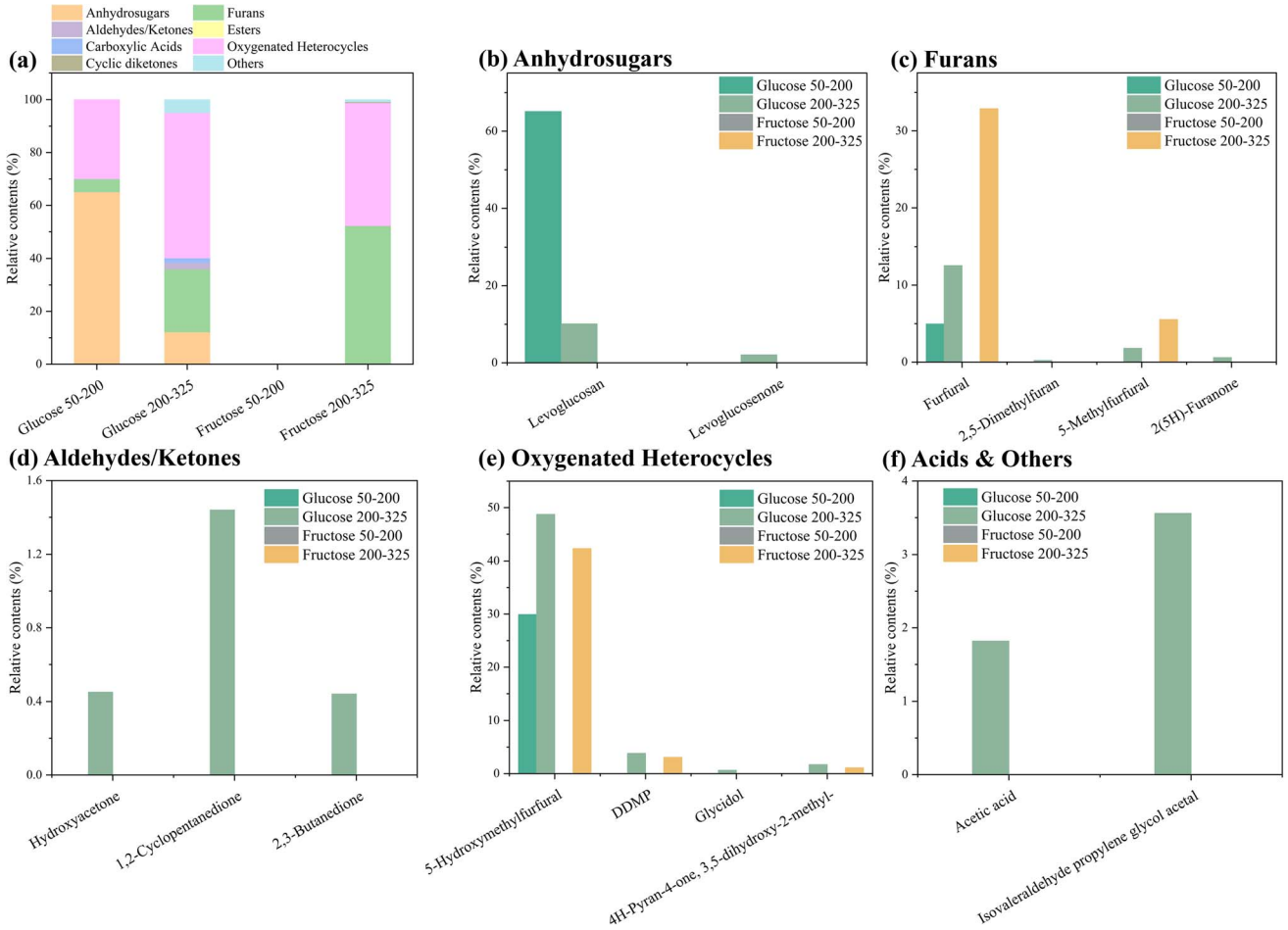

Fig. 2 Product distributions after the temperature-programmed pyrolysis of small-molecule sugars: (a) overall product distributions of glucose and fructose in different temperature ranges; (b) anhydrosugars; (c) furans; (d) aldehydes/ketones; (e) oxygenated heterocycles; (f) acids and other compounds.

progressive transformation from the anhydrosugars to the furan derivatives and back to pure anhydrosugars. When the pyrolysis temperature increased to 200–325 °C, HMF became the predominant product (48.74%), serving as a characteristic marker for this intermediate temperature range, while LVG yield decreased to 10.12%. Remarkably, no detectable products were observed in the 300–500 °C range.

This temperature-dependent product evolution reveals distinct reaction mechanisms: at lower temperatures (50–00 °C), glucose primarily undergoes dehydration to form stable intermediates such as 1,6-anhydroglucopyranose, while higher temperatures (200–325 °C) promote diversified products through ring-opening, isomerization, and multi-step dehydration pathways. Compared to fast pyrolysis, the temperature-programmed approach significantly reduced the yield of small carbonyl compounds, suggesting altered reaction kinetics.[29,30]

The temperature-dependent pyrolysis behavior of fructose exhibited distinct characteristics across different thermal regimes. During the low-temperature phase (50–200 °C), fructose primarily underwent dehydration without yielding detectable volatile products. In contrast, under programmed pyrolysis conditions (200–325 °C), fructose demonstrated remarkable selectivity toward furans, accounting for 90.74% of the total products. The predominance of 5-hydroxymethylfurfural (42.35%) and furfural (32.90%) clearly indicated the facile formation of furan derivatives through dehydration pathways in this temperature range. Additional evidence for diverse furan formation routes was provided by the generation of 2,5-diformylfuran (7.93%) and 5-methylfurfural (5.54%). The presence of 2,3-dihydro-3,5-dihydroxy-6-methyl-4*H*-pyran-4-one (DDMP, 3.08%), a characteristic oxygenated heterocyclic byproduct, suggested the occurrence of radical recombination processes during fructose pyrolysis. Particularly noteworthy was the detection of bis(5-formylfurfuryl) ether (4.82%), implying condensation reactions among furanic aldehydes. Comparative analysis with glucose pyrolysis under identical conditions revealed fructose's superior selectivity for furan production (90.74% *versus* 67.78%) and significantly higher HMF yield (42.35% *versus* 29.92%), which can be mechanistically attributed to the inherent ketose structure of fructose that facilitates 1,2-enolization reactions. This structural advantage enables more efficient conversion to furan derivatives compared to the aldose configuration of glucose.

3.3 Mechanism of fast pyrolysis for macromolecular sugar compounds

As shown in Fig. 3, cellulose pyrolysis at 500 °C primarily yields anhydrosugars (54.53%), dominated by LVG, which is characteristic of cellulose depolymerization. Compared to glucose/fructose pyrolysis, cellulose produces significantly more LVG due to its linear polymer structure. Furans (14.12%), including 5-HMF (7.29%) and furfural (4.96%), form through secondary dehydration reactions but at lower levels than monosaccharide pyrolysis. The presence of small aldehydes/ketones (6.90%), such as glyoxal (5.64%), suggests C–C bond cleavage, while esters (7.68%) (*e.g.*, methylglyoxalate) imply methyl-assisted stabilization of fragments. Cyclic diketones (4.27%) and other heterocycles (3.74%) indicate ring-forming reactions. Maltotriose (7.13%) and DDMP (0.28%) are unique to cellulose, likely from incomplete depolymerization. The absence of acetic acid contrasts with the data for glucose/fructose, highlighting cellulose's lack of acetyl groups.

Amylose exhibits distinct structural characteristics from cellulose; it primarily consists of glucose units linked by α-1,4 glycosidic bonds. This structural difference fundamentally determines their divergent pyrolytic behaviors. During fast pyrolysis at 500 °C, amylose mainly produces anhydrosugars (62.21%), with levoglucosan (58.35%) as the dominant product, formed in significantly higher amounts than during cellulose pyrolysis (54.53%). This demonstrates that the linear structure of amylose facilitates depolymerization into anhydrosugars. The presence of D-mannose (3.86%) may originate from the limited branching points in the amylose structure. Furans (11.62%), mainly 5-hydroxymethylfurfural (6.87%), are formed in lower yields than cellulose (14.12%), indicating weaker dehydration capability. While small aldehydes/ketones (4.71%) and esters (4.52%) exhibit similar proportions to cellulose, the significant presence of maltotriose (9.35%) suggests incomplete depolymerization of the oligosaccharide structures. Collectively, amylose pyrolysis favors the formation of anhydrosugars over furan derivatives, attributable to its highly ordered helical conformation.[31]

Xylan pyrolysis at 500 °C displays characteristic product distribution patterns. Furans (40.45%) dominate, with furfural (31.66%) as the predominant product, which is a consequence of its pentose-based structure as a primary hemicellulose component. Anhydrosugars (34.31%) consist mainly of 1,4-anhydro-D-xylopyranose (19.84%) and LVG (14.47%), revealing concurrent pathways of anhydrosugar formation and glycosidic bond cleavage. The relatively high yield of small carbonyl compounds (12.32%), including methylglyoxal (5.18%) and

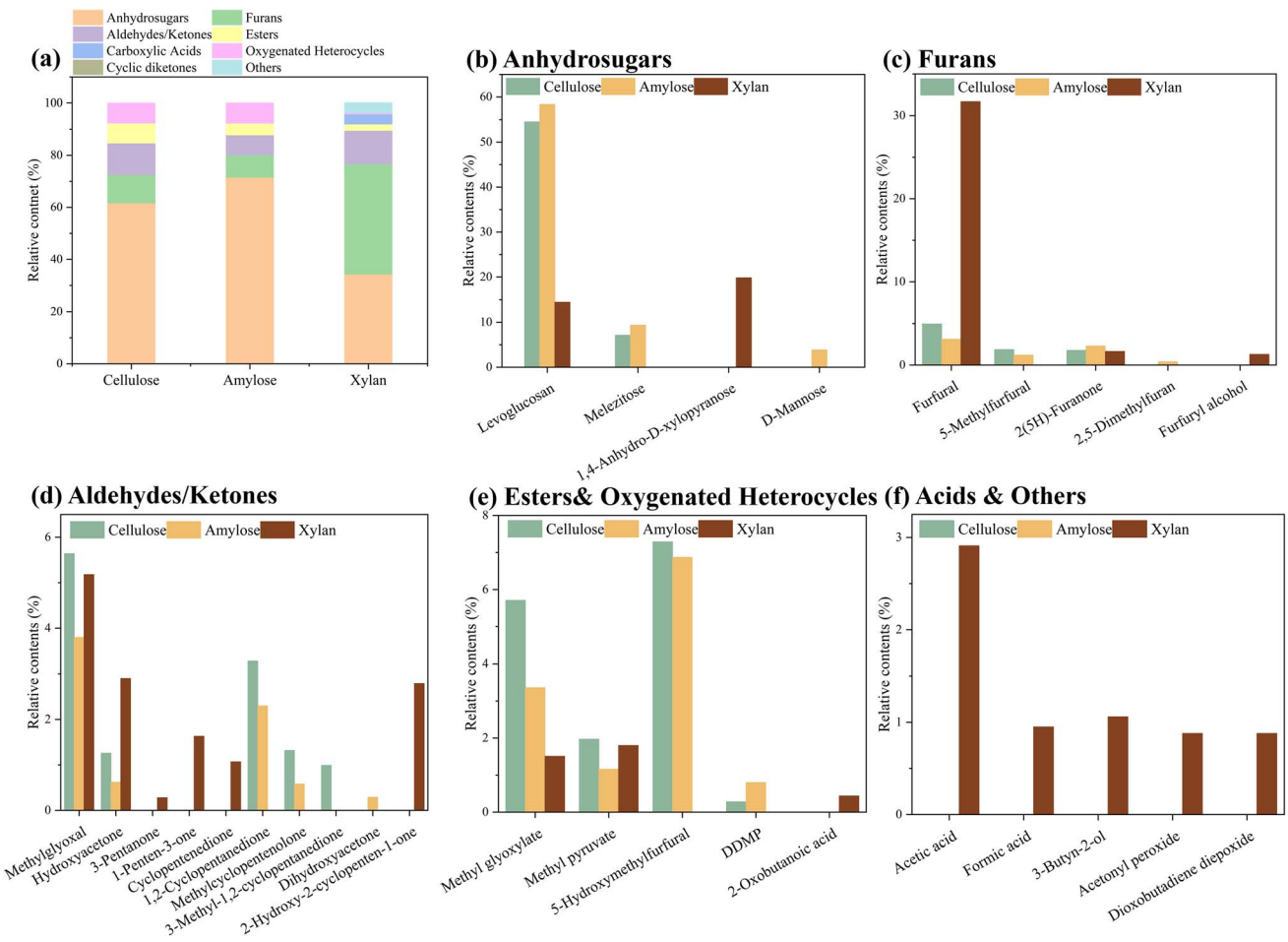

Fig. 3 Product distributions after the fast pyrolysis of macromolecular sugar compounds: (a) overall product distributions of cellulose, amylose and xylan; (b) anhydrosugars; (c) furans; (d) aldehydes/ketones; (e) esters and oxygenated heterocycles; (f) acids and other compounds.

hydroxyacetone (2.90%), reflects active C–C bond scission. Carboxylic acids (3.86%), represented by acetic acid (2.91%), likely derive from acetyl group decomposition. Notably, the presence of specialized heterocycles such as 2(3*H*)-furanone derivatives (6.79%) demonstrates the complexity of xylan pyrolysis pathways. Compared to cellulose, xylan shows a stronger propensity for furan production rather than anhydrosugars, consistent with its amorphous nature and pentose-rich composition.[32]

3.4 Mechanism of temperature-programmed pyrolysis for macromolecular sugar compounds

Fig. 4 shows products from the temperature-programmed pyrolysis of three polysaccharides. Most changes occur at 200–325 °C. Cellulose pyrolysis under these conditions exhibited diversified product distribution, dominated by furans (47.02%), including 5-hydroxymethylfurfural (27.93%) and furfural (8.12%), indicating pronounced dehydration and cyclization tendencies. Oxygenated heterocycles are 20.63% and cyclic diketones are 9.51%. These values indicate ring formation and secondary reactions. The minimal anhydrosugars yield (0.90%), contrasting sharply with high-temperature (325–500 °C) LVG-dominated profiles, suggested preferential chain scission over depolymerization in this regime. Small-molecule products (carbonyls 8.98%, carboxylic acids 3.07%) represented primary cleavage fragments, collectively indicating the suitability of this temperature range for targeted furan production, albeit requiring control over heterocyclic byproducts.

Amylose demonstrated distinct product characteristics, with anhydrosugars (30.91%) predominating through LVG (24.06%) and 1,4,3,6-dianhydroglucopyranose (6.85%), highlighting preserved glycosidic bond cleavage capacity. Its lower furan yield (22.94% *versus* 47.02% for cellulose) reflected structural inhibition on furan formation, while the distinctive cyclopropyl methanol (23.88%) suggested unique ring-opening pathways. The maintained anhydrosugars preference (30.91% *vs.* 0.90% for cellulose) established optimal conditions for LVG production.

Xylan exhibited exceptional furan selectivity (55.87%), overwhelmingly featuring furfural (46.6%) due to pentose-unit

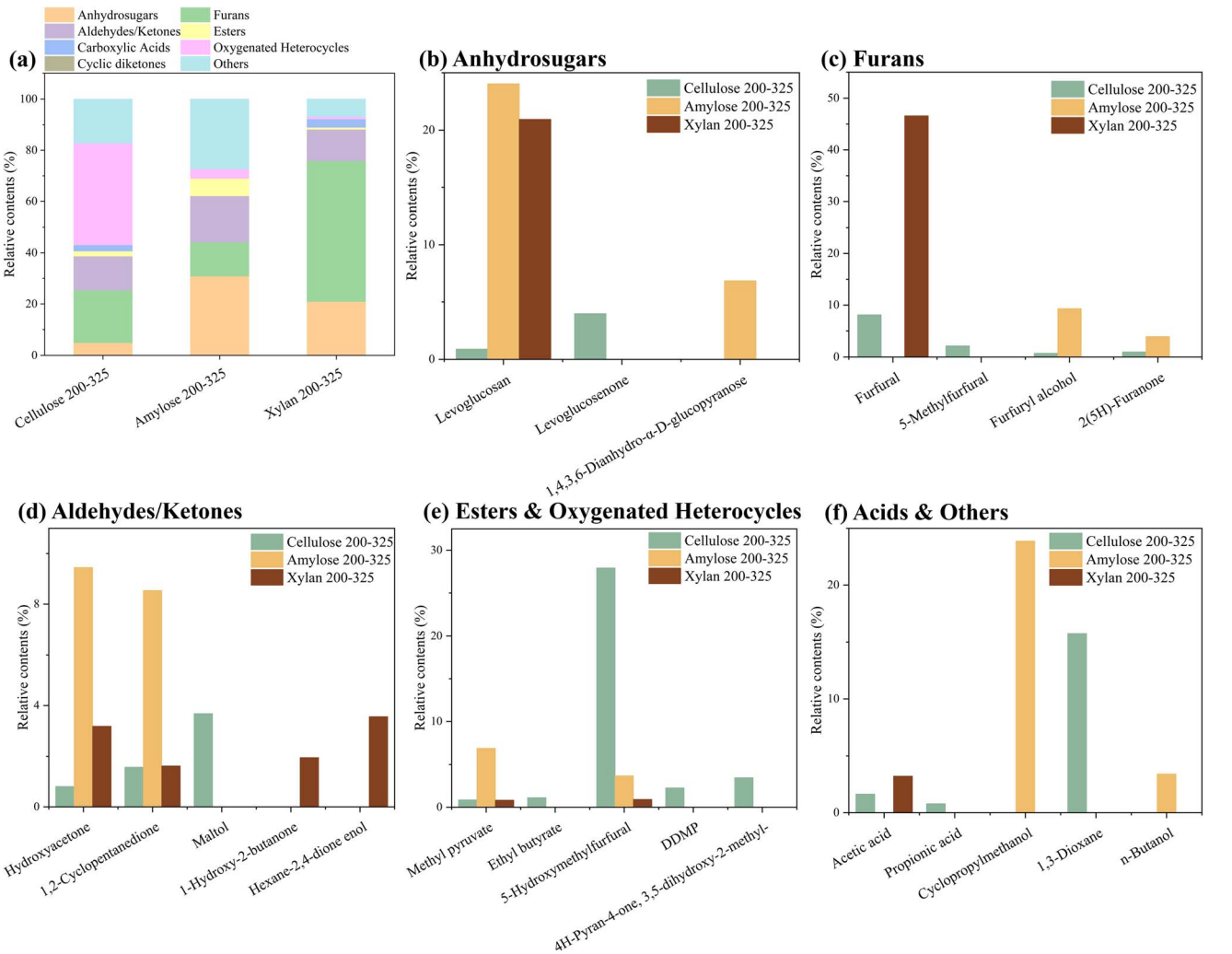

Fig. 4 Product distributions after the temperature-programmed pyrolysis of macromolecular sugar compounds: (a) overall product distributions of cellulose, amylose and xylan; (b) anhydrosugars; (c) furans; (d) aldehydes/ketones; (e) esters and oxygenated heterocycles; (f) acids and other compounds.

reactivity, alongside characteristic 4-hydroxy-5-methyl-3(2*H*)-furanone (8.35%). Its residual glucose-unit depolymerization capacity (LVG 15.11%) and minimal HMF production (0.92%) contrasted sharply with cellulose, offering superior furfural selectivity.

The observed differences in pyrolytic behavior fundamentally stem from the distinct structural characteristics of each polysaccharide. Cellulose's β-1,4 glycosidic linkages, combined with its amorphous regions, preferentially facilitate dehydration and cyclization reactions. This phenomenon can be attributed to the fact that cellulose first undergoes glycosidic bond cleavage, after which the terminal glucose units undergo intramolecular dehydration and cyclization to form LVG. In contrast, xylan lacks a similar structural pathway and therefore tends to undergo direct dehydration to yield furfural. Compared with fast pyrolysis (furans 8.61%, anhydrosugars 54.53%), the 200–325 °C programmed window raises furans and 5-HMF to 39.89% and lowers anhydrosugars to 0.90%, indicating the dominance of dehydration and cyclization over depolymerization to anhydrosugars. Amylose's α-1,4 bonded helical configuration promotes intramolecular dehydration pathways. Anhydrosugars accounted for 71.56% of the products under fast pyrolysis, whereas under temperature-programmed pyrolysis at 200–325 °C they accounted for 30.91%, indicating that depolymerization and dehydration–cyclization pathways are sensitive to the pyrolysis heating rate. Amylose preferentially yields aldehydes and ketones under temperature-programmed pyrolysis. In contrast, xylan's pentose-based amorphous molecular architecture preferentially enables 1,2-dehydration mechanisms. The proportion of furans increased from 34.61% (fast pyrolysis) to 54.95% (temperature-programmed pyrolysis), while furfural rose from 31.66% to 46.60%, indicating that dwelling at intermediate temperatures promotes more pronounced pentose-driven dehydration. Macromolecular sugars such as cellulose typically undergo pyrolytic reactions (particularly under fast pyrolysis conditions) to produce LVG, whereas small-molecule sugars such as glucose are more prone to fragmentation reactions, yielding small furans and carbonyl compounds. These divergent thermal decomposition pathways—ranging from depolymerization to fragmentation—are collectively governed by two critical structural factors: the relative crystallinity/amorphous ratio of the polymer matrix and the specific monosaccharide composition of each polysaccharide.[33] The interplay between these structural parameters ultimately determines the dominant reaction channels during thermal decomposition, accounting for the distinct product distributions observed among the three carbohydrate polymers.

3.5 Mechanism of the Maillard reaction under fast pyrolysis

Investigating the Maillard reaction of sugars holds significant implications for understanding tobacco pyrolysis mechanisms. As a non-enzymatic reaction between reducing sugars and nitrogen-containing compounds (*e.g.*, amino acids, proteins) under thermal conditions, the Maillard reaction occurs ubiquitously during tobacco processing and pyrolysis.[14,34] This reaction generates flavor compounds and regulates the network, shaping smoke aroma and composition. Building upon previous research foundations, we designed pyrolysis experiments with a sugar-to-amino acid molar ratio of 6 : 1, based on the typical content of small-molecule sugars and amino acids in tobacco leaves, followed by comprehensive product analysis.

Fig. 5 illustrates the product distribution of Maillard reactions involving small-molecule sugars under fast pyrolysis conditions (500 °C). The glucose–proline system exhibited distinct characteristics, with small carbonyl compounds (41.59%) dominating the product profile, particularly 2,3-butanedione (34.99%) as the primary product, representing typical α-dicarbonyl formation pathways in Maillard chemistry. Carboxylic acids (22.54%), predominantly acetic acid (22.54%), likely originated from both sugar fragmentation and amino acid decarboxylation. Furans (16.33%), including 2,5-dimethylfuran (6.68%), furfural (5.44%), and 5-methylfurfural (4.21%), demonstrated sugar dehydration and cyclization processes. The presence of esters (7.58%) and cyclic diketones/ketols (9.47%) further confirmed the reaction complexity, involving secondary pathways such as Strecker degradation and cyclization. Notably, *N*,*N*-diethylaniline (2.48%) indicated nitrogenous heterocycle formation through proline participation. Compared to pure glucose pyrolysis, the Maillard reaction significantly enhanced small carbonyl and nitrogen-containing compound yields (by 3.2- and 2.8-fold, respectively), demonstrating amino acid-directed pathway regulation.

The fructose-proline system displayed contrasting features: carboxylic acids (22.12%, mainly acetic acid) reflected substantial degradation/decarboxylation, while small carbonyls (20.52%) were dominated by hydroxyacetone, indicating preferential α-hydroxy ketone formation from the ketose structure. Remarkably high ester content (19.45%), including ethyl glycolate (12.38%) and methyl 2-oxopropanoate (7.07%), highlighted active esterification. Although furans (23.64%) showed lower abundance than in the glucose systems, the diversity of nitrogenous heterocycles (4.65%), particularly pyrrolidine derivatives, and *N*,*N*-diethylaniline (2.57%) confirmed the extensive involvement of proline.

The observed distinctions between the glucose and fructose Maillard reaction systems under fast pyrolysis conditions primarily stem from their inherent structural differences in sugar configuration. Fructose's ketose structure exhibits a 2.6-fold greater ester formation compared to glucose, along with more diversified nitrogen-containing heterocycles such as 1-(1′-pyrrolidinyl)-2-propanone, while glucose demonstrates 1.7-fold higher selectivity toward furans. These differential product distributions can be mechanistically explained by the preferential reaction pathways enabled by the molecular architecture of each sugar.[35] The ketose configuration of fructose preferentially undergoes 2,3-enolization, leading to enhanced fragmentation and subsequent formation of ester derivatives through recombination with proline-derived intermediates.[35,36] Glucose's aldose structure favors 1,2-enolization pathways that promote cyclic condensation reactions, resulting in greater furan production. The more varied nitrogenous heterocycles in the fructose system arise from its greater propensity for

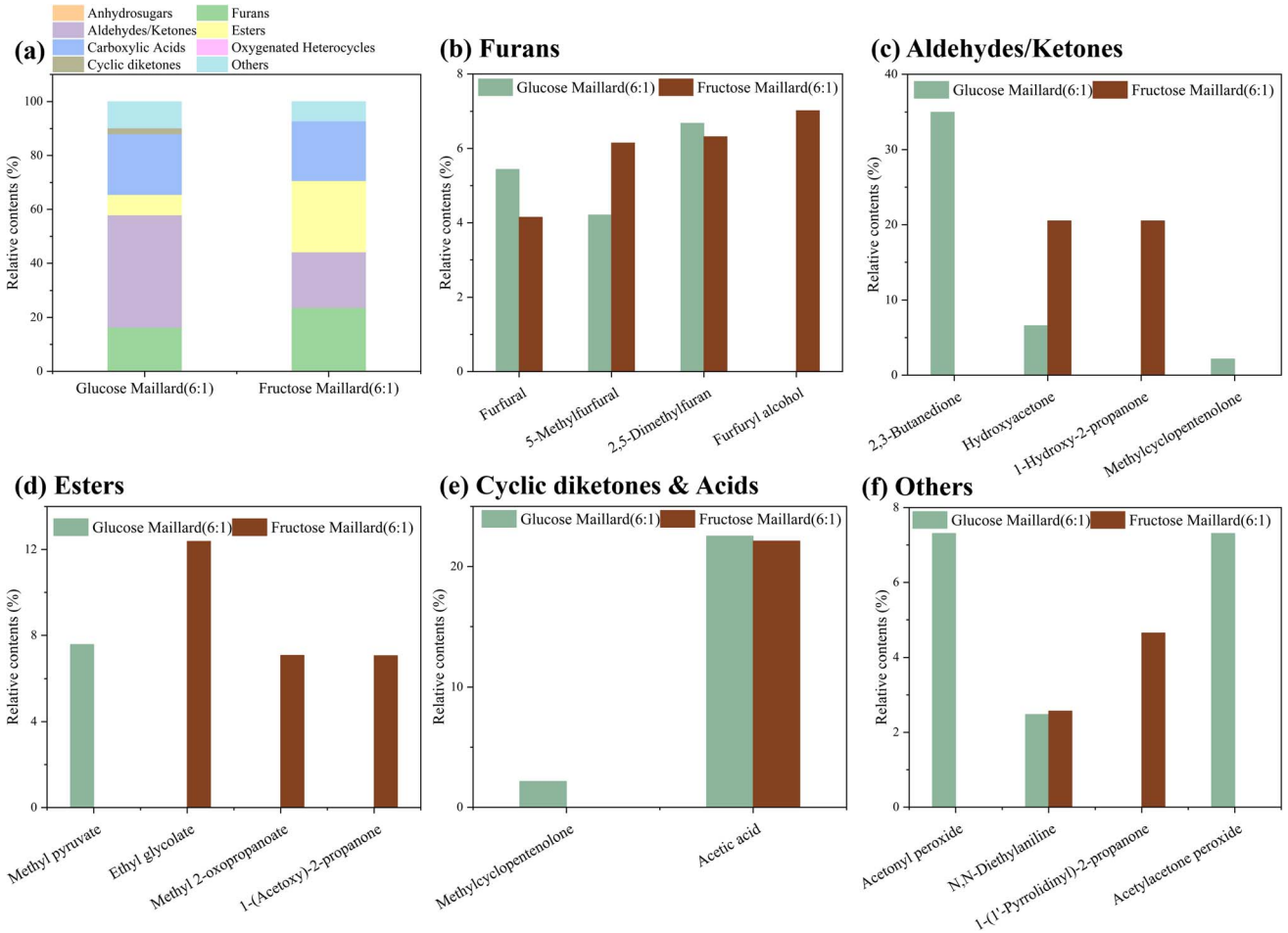

Fig. 5 Product distributions after the Maillard reaction under fast pyrolysis: (a) overall product distributions of glucose Maillard (6 : 1) and fructose Maillard (6 : 1) systems; (b) furans; (c) aldehydes/ketones; (d) esters; (e) cyclic diketones and acids; (f) other compounds.

fragmentation, which provides a wider array of reactive carbonyl intermediates for condensation with amino acid decomposition products. The incorporation of proline redirects the pyrolysis pathway of carbohydrate toward the Maillard reaction route. Nitrogen-containing heterocyclic compounds are formed in accordance with the classical Maillard reaction mechanism, even under pyrolytic conditions. During the co-pyrolysis of amino acids and fructose, free ammonia released from amino acid deamination rapidly condenses with aldehydes generated from sugar cleavage, resulting in the formation of substituted pyrazines.

3.6 Mechanism of the Maillard reaction under temperature-programmed pyrolysis

As shown in Fig. 6, the temperature-programmed Maillard reaction of glucose with proline exhibited distinct stage-dependent product distributions. In the low-temperature range (50–200 °C), oxygenated heterocycles dominated (69.45%), with DDMP as the major product (65.02%), indicating preferential formation of pyranone derivatives through 1,2-enolization pathways. Carboxylic acids accounted for 25.28% (mainly acetic acid, 23.57%), suggesting significant sugar fragmentation and amino acid decarboxylation. At higher temperatures (200–325 °C), the product profile shifted dramatically to furans (87.48%), predominantly 2,5-dimethylfuran (73.73%) and furyl acetone derivatives (13.75%), demonstrating the thermal activation of dehydration and cyclization pathways.

Fructose-proline Maillard reaction showed contrasting behavior, with carboxylic acids maintaining high yields across both temperature ranges (31.90% at 50–200 °C; 34.01% at 200–325 °C). The low-temperature stage produced more diversified products, including significant amounts of furans (14.78%, with 6.78% furfural) and oxygenated heterocycles (49.46%, mainly DDMP at 44.35%). Notably, 5-HMF appeared at 4.26%, reflecting fructose's inherent tendency for furanose formation. The high-temperature phase exhibited enhanced furan production (42.49%), albeit with different selectivity (28.07% 2,5-dimethylfuran *vs.* 73.73% for glucose), along with substantial nitrogenous byproducts.

The comparative analysis between glucose and fructose Maillard reactions reveals fundamental differences in their reaction mechanisms and product distributions, primarily stemming from their distinct sugar configurations. Glucose demonstrates more concentrated product formation, particularly in high-temperature furan production (87.48% *versus* 42.49% for fructose), reflecting its tendency for selective

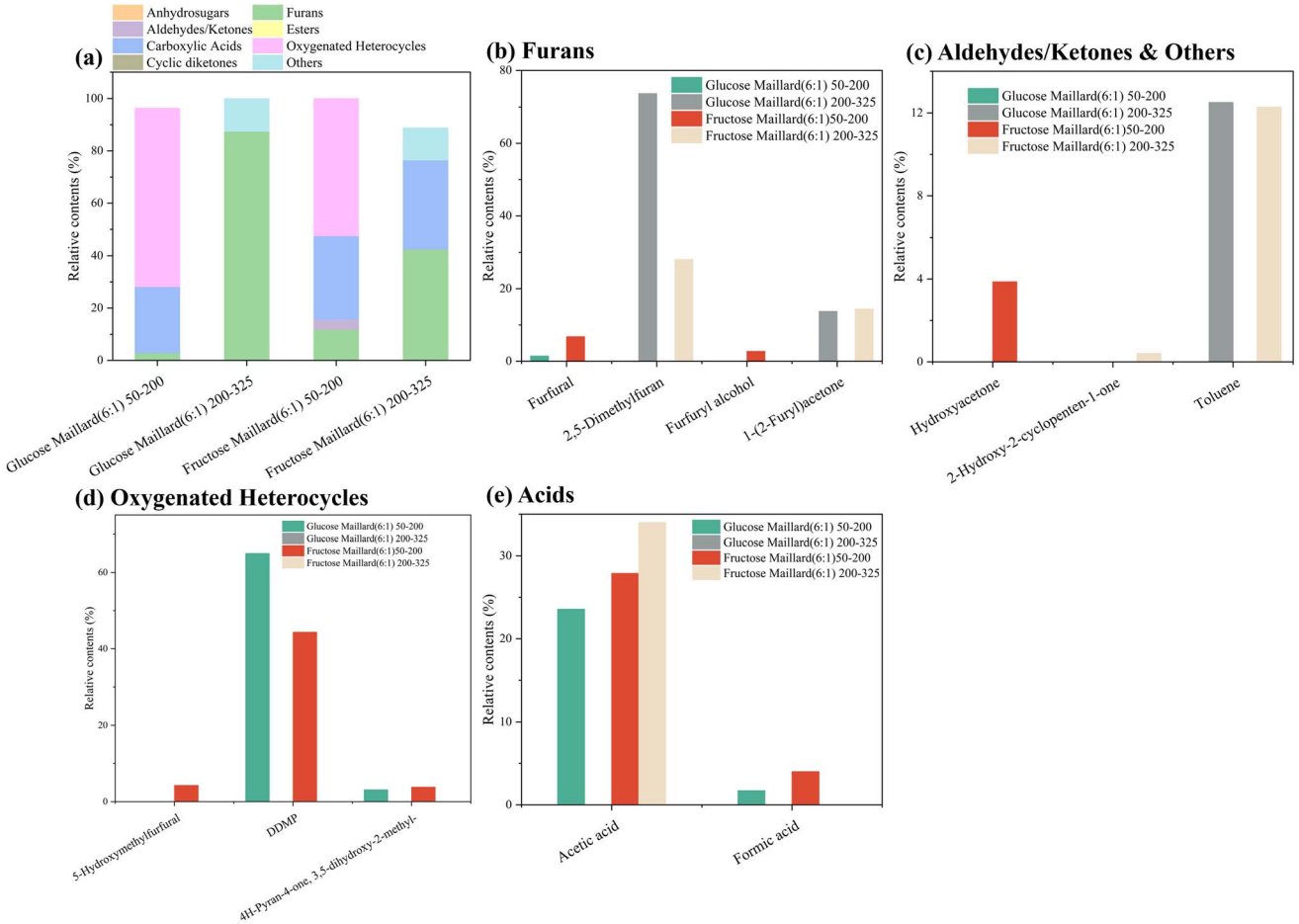

Fig. 6 Product distributions after the Maillard reaction under temperature-programmed pyrolysis: (a) overall product distribution of glucose Maillard and fructose Maillard systems; (b) furans; (c) aldehydes/ketones; (d) esters; (e) cyclic diketones and acids; (f) other compounds.

cyclization pathways, while fructose maintains greater product diversity due to its enhanced fragmentation propensity.[37,38] This mechanistic divergence is further evidenced by fructose's consistently higher carboxylic acid yields (31.90–34.01% compared to 25.28% for glucose), which aligns with its known thermal lability and greater susceptibility to chain scission. The characteristics of the dominant products further underscore these differences; glucose preferentially forms compact furan structures, such as 2,5-dimethylfuran, through efficient ring closure, whereas fructose generates more functionalized derivatives, such as furyl acetone, through its propensity for side-chain retention.[39] Particularly revealing is the significant disparity in DDMP yields (65.02% for glucose *versus* 44.35% for fructose), which serves as a clear indicator of their distinct enolization pathways: glucose's aldose structure favors 1,2-enolization leading to pyranone derivatives, while fructose's ketose configuration promotes 2,3-enolization that competes with DDMP formation.

Maillard chemistry reorganizes the pyrolysis of glucose and fructose. For glucose, adding proline introduces nitrogenous products (12.51%) and suppresses anhydrosugars (LVG 65.12% → 0%). The amino acid interaction also promotes earlier furan generation (1.45% at 50–200 °C compared to none in pure glucose) and alters high-temperature product selectivity (87.48% furans *versus* 67.78%). Similarly, the fructose Maillard system undergoes substantial transformation from its pure pyrolysis behavior, exhibiting amplified carboxylic acid production (1.5–1.8× increase) and dramatic suppression of HMF yield (8-fold reduction to 4.26%), alongside complete elimination of high-temperature anhydrosugars. The introduction of nitrogenous compounds (23.50%) and reduction in overall furan selectivity (42.49% *versus* 90.74%) reveal how amino acid involvement competes with and disrupts fructose's inherent dehydration pathways, favoring fragmentation processes over cyclization. These parallel yet distinct modifications in both sugar systems highlight the profound influence of Maillard chemistry in restructuring thermal decomposition networks, where amino acids not only contribute nitrogen incorporation but also fundamentally alter the balance between fragmentation, dehydration, and recombination pathways through their catalytic and competitive interactions with sugar decomposition intermediates.

The product distribution of the Maillard reaction is highly sensitive to temperature and heating rate. Temperature-programmed systems promote the formation and accumulation of specific intermediates, whereas fast pyrolysis often

bypasses or rapidly cleaves these intermediates, yielding distinct product slates. Hosry *et al.*[40] reported that pyrolysis of Maillard-derived Amadori compounds at 300 °C affords detectable intermediates, while these intermediates fully decompose at 700 °C into smaller volatile products. Temperature-programmed pyrolysis experiments captured stepwise reaction features absent under fast pyrolysis. This behavior conforms to general pyrolysis trends: fast pyrolysis favors volatile products, whereas slower heating or longer residence times facilitate secondary reactions that generate heavier products. At higher temperatures, fragmentation pathways in the Maillard network accelerate, producing more small molecules while larger intermediates are short-lived; by contrast, lower temperatures favor the buildup of early-stage products such as Amadori-rearrangement species and cyclic diketones. Practically, fast pyrolysis drives the network rapidly into deep-dehydration regimes, while gradual heating permits the generation and subsequent transformation of intermediates (*e.g.*, DDMP), thereby broadening product diversity.

4 Conclusion

This study elucidates the structure-dependent pyrolysis mechanisms of tobacco carbohydrates, revealing how small-molecule sugars (glucose and fructose) and polysaccharides (cellulose, amylose, and xylan) exhibit distinct product profiles governed by their specific glycosidic linkages, monosaccharide composition, and crystallinity. Glucose's aldose structure promotes 1,2-enolization pathways that yield balanced furan and pyran derivatives, while fructose's ketose configuration drives preferential 2,3-enolization, resulting in enhanced furan production (*e.g.*, 34.27% 5-HMF) and fragmentation products. For polysaccharides, cellulose's linear β-1,4-glycosidic bonds facilitate LVG formation (54.53%), whereas amylose's helical α-1,4-linked structure significantly increases anhydrosugar yields (62.21%), and xylan's amorphous pentose units selectively generate furfural (46.6%) through 1,2-dehydration pathways. Maintaining the temperature within 200–325 °C generally enriches furan-type products while suppressing anhydrosugars, whereas fast pyrolysis at 500 °C favors anhydrosugars and light carbonyls. These trends demonstrate that temperature-programmed pyrolysis enables controllable tuning of the competition between dehydration–cyclization and polycondensation pathways of carbohydrate-derived intermediates. The introduction of proline in Maillard reactions dramatically redirects these pyrolysis pathways toward nitrogenous heterocycles (12.51%) and esters (19.45% for fructose), while suppressing anhydrosugar formation and modifying furan selectivity. For carbohydrate compounds, different pyrolysis methods exhibit distinct product distribution characteristics. Temperature-programmed pyrolysis enhances the generation of furans while suppressing anhydrosugars, whereas fast pyrolysis tends to favor small carbonyl species. In particular, temperature-programmed pyrolysis exhibits greater selectivity toward furans and 2,5-dimethylfuran, while fast pyrolysis is more conducive to the formation of HMF. These findings provide fundamental insights into the critical relationship between carbohydrate structure and pyrolysis chemistry, offering practical approaches to optimize tobacco pyrolysis for targeted aroma profile development through controlled thermal processing. Future investigations should explore synergistic effects during co-pyrolysis with other tobacco components, such as lignin and proteins, to further advance reaction precision and product control.

Author contributions

Yuhan Peng: writing – original draft, investigation. Xiaopeng Shi: writing – original draft, investigation conceptualization, data curation. Xiaodong Tang: data curation. Lu Dai: investigation. Depo Cao: investigation. Qingxiang Li: resources. Fangqi Du: resources. Kaige Wang: resources. writing – reviewing and editing. Yiming Bi: writing – reviewing and editing.

Conflicts of interest

There are no conflicts to declare.

Data availability

The data for this article have been included in the manuscript.

All data are available in the article and the supplementary information (SI) (raw product distributions, representative GC/MS chromatograms and experimental details). Supplementary information: additional data and materials supporting this study, including (i) GC/MS chromatograms for glucose and cellulose under both fast pyrolysis and temperature-programmed conditions (Fig. S1–S6); (ii) tabulated product distributions for fast pyrolysis of sugar compounds (glucose, fructose, cellulose, amylose, and xylan) (Table S1); (iii) product distributions for temperature-programmed pyrolysis of small-molecule sugars (glucose and fructose; 50–200 °C and 200–325 °C) (Table S2); (iv) product distributions for temperature-programmed pyrolysis of macromolecular sugar compounds (cellulose, amylose, and xylan; 200–325 °C) (Table S3); and (v) product distributions for Maillard reaction systems under fast pyrolysis and temperature-programmed conditions (Tables S4 and S5). See DOI: https://doi.org/10.1039/d5ra07210g.

Acknowledgements

The authors acknowledge Zhejiang China Tobacco Co., Ltd. Science and Technology Project (No. ZJZY2023C020).

References

1 A. K. Maiyo, J. K. Kibet and F. O. Kengara, A review of the characteristic properties of selected tobacco chemicals and their associated etiological risks, *Rev. Environ. Health*, 2023, **38**(3), 479–491, DOI: 10.1515/reveh-2022-0013.

2 R. A. W. Johnstone and J. R. Plimmer, The Chemical Constituents Of Tobacco And Tobacco Smoke, *Chem. Rev.*, 1959, **59**(5), 885–936, DOI: 10.1021/cr50029a004.

3 S. Liao, L. Zhu, J. Xu, J. Jiang, G. Zhou and S. Wang, Study on the effect of different solvent pretreatment on the pyrolysis characteristics of tobacco, *J. Anal. Appl. Pyrolysis*, 2023, **174**, 106142, DOI: 10.1016/j.jaap.2023.106142.

4 C. Ma, F. Zhang, H. Liu, J. Hu, S. Yang and H. Wang, Comprehensive investigation on the slow pyrolysis product characteristics of waste tobacco stem: Pyrolysis reaction mechanism and conversion mechanism of N, *Fuel*, 2023, **350**, 128902, DOI: 10.1016/j.fuel.2023.128902.

5 L. Zhu, J. Xu, Y. Dai, J. Jiang, S. Liao, G. Zhou and S. Wang, Mechanism study of tobacco pyrolysis based on the analysis of characteristic products and in-situ identification of functional groups evolution on pyrolytic char, *J. Anal. Appl. Pyrolysis*, 2022, **167**, 105681, DOI: 10.1016/j.jaap.2022.105681.

6 J. Ramontja, K. O. Iwuozor, E. C. Emenike, C. J. Okorie, H. B. Saka, A. O. Ezzat, J. A. Adeleke, O. D. Saliu and A. G. Adeniyi, From tobacco to biochar: a review of production processes, properties, and applications, *Biofuel Bioprod. Biorefining*, 2025, **19**(3), 911–928, DOI: 10.1002/bbb.2728.

7 Z. Zhu, C. Zhang, Y. Shi, P. Zou, N. Ding, K. Zong, L. Jia and D. Guo, Fast Pyrolysis of Cigarette and Cigar Leaves: Differential Analysis of Their Heavy Products by Ultrahigh-Resolution Mass Spectrometry, *Rapid Commun. Mass Spectrom.*, 2025, **39**(10), e10011, DOI: 10.1002/rcm.10011.

8 M. Liang, Y. Wang, S. Dai, L. Hong, R. Li, Z. Xu, J. Su and J. Zhang, Effect of glycerol addition and heating rate on the thermal release behavior of cigar tobacco, *Biomass Convers. Biorefinery*, 2025, **15**(4), 6071–6086, DOI: 10.1007/s13399-024-05484-7.

9 Z. He, A. Zhao, S. Liu, Y. Chen, J. Liu, W. Zhao, M. Yin, Q. Dong, J. Zhang, G. Zhang, *et al.*, Preparation of nitrogen-containing chemicals from lignocellulosic biomass and nitrogen-rich organic solid waste by pyrolysis: Characteristics, reaction mechanisms, and feedstock interactions, *Chem. Eng. J.*, 2024, **496**, 153793, DOI: 10.1016/j.cej.2024.153793.

10 J. Bai, L. Li, Z. Chen, C. Chang, S. Pang and P. Li, Study on the optimization of hydrothermal liquefaction performance of tobacco stem and the high value utilization of catalytic products, *Energy*, 2023, **281**, 128283, DOI: 10.1016/j.energy.2023.128283.

11 J. Li, Z. Ma, H. Dai, H. Li, J. Qiu and X. Pang, Application of PLSR in correlating sensory and chemical properties of middle flue-cured tobacco leaves with honey-sweet and burnt flavour, *Heliyon*, 2024, **10**(8), DOI: 10.1016/j.heliyon.2024.e29547.

12 N. S. Hassan, A. A. Jalil, C. N. C. Hitam, D. V. N. Vo and W. Nabgan, Biofuels and renewable chemicals production by catalytic pyrolysis of cellulose: a review, *Environ. Chem. Lett.*, 2020, **18**(5), 1625–1648, DOI: 10.1007/s10311-020-01040-7.

13 S. Krishnan-Sarin, S. S. O'Malley, B. G. Green and S. E. Jordt, The science of flavour in tobacco products, *W. H. O. Tech. Rep. Ser.*, 2019, **1015**, 125–142.

14 J. Bai, H. Gao, J. Xu, L. Li, P. Zheng, P. Li, J. Song, C. Chang and S. Pang, Comprehensive study on the pyrolysis product characteristics of tobacco stems based on a novel nitrogen-enriched pyrolysis method, *Energy*, 2022, **242**, 122535, DOI: 10.1016/j.energy.2021.122535.

15 H. Cheng, J. Wang and J. Xie, Progress on odor deterioration of aquatic products: Characteristic volatile compounds, analysis methods, and formation mechanisms, *Food Biosci.*, 2023, **53**, 102666, DOI: 10.1016/j.fbio.2023.102666.

16 O. Debono and A. Villot, Nitrogen products and reaction pathway of nitrogen compounds during the pyrolysis of various organic wastes, *J. Anal. Appl. Pyrolysis*, 2015, **114**, 222–234, DOI: 10.1016/j.jaap.2015.06.002.

17 J. Xiong, S. Zhang, L. Ke, Q. Wu, Q. Zhang, X. Cui, A. Dai, C. Xu, K. Cobb, Y. Liu, *et al.*, Research progress on pyrolysis of nitrogen-containing biomass for fuels, materials, and chemicals production, *Sci. Total Environ.*, 2023, **872**, 162214, DOI: 10.1016/j.scitotenv.2023.162214.

18 Z. Guo, K. Zhang, Q. Zhang, L. Fu, Z. Liu, Z. Kong, L. Wang, C. Liu, L. Hua and B. Li, Tobacco fractionation and its effects on pyrolysis chemistry, *J. Anal. Appl. Pyrolysis*, 2022, **167**, 105650, DOI: 10.1016/j.jaap.2022.105650.

19 H. Wang, W. Xia, H. Yu, H. Chen, Y. Pan, Y. Sun, S. Li and S. Han, A theoretical investigation on the transformer oil pyrolysis mechanism and the effect of the small molecule acid in oils, *Fuel*, 2024, **361**, 130522, DOI: 10.1016/j.fuel.2023.130522.

20 F. Mao, H. Fan and J. Wang, Biogenic oxygenates in lignite pyrolysis tars and their thermal cracking revealed by two-dimensional gas chromatography/time-of-flight mass spectrometry (GC×GC-TOFMS), *J. Anal. Appl. Pyrolysis*, 2019, **139**, 213–223, DOI: 10.1016/j.jaap.2019.02.008.

21 C. Li, Y. Sun, D. Dong, G. Gao, S. Zhang, Y. Wang, J. Xiang, S. Hu, G. Mortaza and X. Hu, Co-pyrolysis of cellulose/lignin and sawdust: Influence of secondary condensation of the volatiles on characteristics of biochar, *Energy*, 2021, **226**, 120442, DOI: 10.1016/j.energy.2021.120442.

22 Y. Wu, Q. Gui, H. Zhang, H. Li, B. Li, M. Liu, Y. Chen, S. Zhang, H. Yang and H. Chen, Effect of biomass components' interaction on the pyrolysis reaction kinetics and small-molecule product release characteristics, *J. Anal. Appl. Pyrolysis*, 2023, **173**, 106039, DOI: 10.1016/j.jaap.2023.106039.

23 Q. Wang, H. Song, S. Pan, N. Dong, X. Wang and S. Sun, Initial pyrolysis mechanism and product formation of cellulose: An Experimental and Density functional theory(DFT) study, *Sci. Rep.*, 2020, **10**(1), 3626, DOI: 10.1038/s41598-020-60095-2.

24 Y. Peng, Y. Tian, Q. Li, S. Li, X. Shi, K. Wang and L. Fu, Influence of Expansion Pretreatment on the Structure Evolution and Reaction Chemistry during Oxidative Pyrolysis of Tobacco Biomass, *ACS Omega*, 2025, **10**(18), 18552–18560, DOI: 10.1021/acsomega.4c11162.

25 A. Nagai, T. Yamamoto and H. Wariishi, Identification of Fructo- and Malto-oligosaccharides in Cured Tobacco Leaves (Nicotiana tabacum), *J. Agric. Food Chem.*, 2012, **60**(26), 6606–6612, DOI: 10.1021/jf301395v.

26 E. Leng, M. Costa, Y. Peng, Y. Zhang, X. Gong, A. Zheng, Y. Huang and M. Xu, Role of different chain end types in pyrolysis of glucose-based anhydro-sugars and oligosaccharides, *Fuel*, 2018, **234**, 738–745, DOI: 10.1016/j.fuel.2018.07.075.

27 C. Chen, M. Lv, H. Hu, L. Huai, B. Zhu, S. Fan, Q. Wang and J. Zhang, 5-Hydroxymethylfurfural and its Downstream Chemicals: A Review of Catalytic Routes, *Adv. Mater.*, 2024, **36**(37), 2311464, DOI: 10.1002/adma.202311464.

28 J. Slak, B. Pomeroy, A. Kostyniuk, M. Grilc and B. Likozar, A review of bio-refining process intensification in catalytic conversion reactions, separations and purifications of hydroxymethylfurfural (HMF) and furfural, *Chem. Eng. J.*, 2022, **429**, 132325, DOI: 10.1016/j.cej.2021.132325.

29 R. Lin, L. Wang, J. Zhang, X. Li, W. Zheng and L. Zhang, Comparative study of temperature-programmed pyrolysis and two-step fast pyrolysis of oily sludge, *J. Anal. Appl. Pyrolysis*, 2023, **173**, 106097, DOI: 10.1016/j.jaap.2023.106097.

30 S. Du, J. A. Valla and G. M. Bollas, Characteristics and origin of char and coke from fast and slow, catalytic and thermal pyrolysis of biomass and relevant model compounds, *Green Chem.*, 2013, **15**(11), 3214–3229, DOI: 10.1039/C3GC41581C.

31 C. Wang, S. Xia, X. Yang, A. Zheng, Z. Zhao and H. Li, Oriented valorization of cellulose and xylan into anhydrosugars by using low-temperature pyrolysis, *Fuel*, 2021, **291**, 120156, DOI: 10.1016/j.fuel.2021.120156.

32 D. O. Usino, Supriyanto, P. Ylitervo, A. Pettersson and T. Richards, Influence of temperature and time on initial pyrolysis of cellulose and xylan, *J. Anal. Appl. Pyrolysis*, 2020, **147**, 104782, DOI: 10.1016/j.jaap.2020.104782.

33 P. A. V. Freitas, L. G. Santana, C. González-Martínez and A. Chiralt, Combining subcritical water extraction and bleaching with hydrogen peroxide to obtain cellulose fibres from rice straw, *Carbohydr. Polym. Technol. Appl.*, 2024, **7**, 100491, DOI: 10.1016/j.carpta.2024.100491.

34 W. Wu, Y. Mei, L. Zhang, R. Liu and J. Cai, Kinetics and reaction chemistry of pyrolysis and combustion of tobacco waste, *Fuel*, 2015, **156**, 71–80, DOI: 10.1016/j.fuel.2015.04.016.

35 S. Datta and S. Bhattacharya, Multifarious facets of sugar-derived molecular gels: molecular features, mechanisms of self-assembly and emerging applications, *Chem. Soc. Rev.*, 2015, **44**(15), 5596–5637, DOI: 10.1039/C5CS00093A.

36 C. E. Suh, H. M. Carder and A. E. Wendlandt, Selective Transformations of Carbohydrates Inspired by Radical-Based Enzymatic Mechanisms, *ACS Chem. Biol.*, 2021, **16**(10), 1814–1828, DOI: 10.1021/acschembio.1c00190.

37 A. Massaro, M. P. Colombini and E. Ribechini, Fructose and inulin: Behaviour under analytical pyrolysis, *J. Anal. Appl. Pyrolysis*, 2016, **121**, 205–212, DOI: 10.1016/j.jaap.2016.07.021.

38 C. Luo, Q. Yin, L. Zeng, Q. Zhang, B. Wang, G. Yu, S. Shen and W. Xie, Insight into co-pyrolysis behavior of asparagine/fructose mixtures using on-line pyrolysis-GC/MS, *J. Anal. Appl. Pyrolysis*, 2025, **186**, 106969, DOI: 10.1016/j.jaap.2025.106969.

39 A. T. Hoang, A. Pandey, Z. Huang, R. Luque, K. H. Ng, A. M. Papadopoulos, W.-H. Chen, S. Rajamohan, H. Hadiyanto, X. P. Nguyen, *et al.*, Catalyst-Based Synthesis of 2,5-Dimethylfuran from Carbohydrates as a Sustainable Biofuel Production Route, *ACS Sustain. Chem. Eng.*, 2022, **10**(10), 3079–3115, DOI: 10.1021/acssuschemeng.1c06363.

40 L. El Hosry, V. Elias, V. Chamoun, M. Halawi, P. Cayot, A. Nehme and E. Bou-Maroun, Maillard Reaction: Mechanism, Influencing Parameters, Advantages, Disadvantages, and Food Industrial Applications: A Review, *Foods*, 2025, **14**(11), 1881.